

(H)ALPing the 511 keV line: A thermal DM interpretation of the 511 keV emission

Mohammad Aghaie,^{1,2} Pedro De la Torre Luque,^{3,4} Alessandro Dondarini,^{1,2,5} Daniele Gaggero,² Giulio Marino,^{1,2} and Paolo Panci^{1,2}

¹*Dipartimento di Fisica “E. Fermi”, Università di Pisa, Largo Pontecorvo 3, 56127 Pisa, Italy*

²*INFN Sezione di Pisa, Polo Fibonacci, Largo B. Pontecorvo 3, 56127 Pisa, Italy*

³*Departamento de Física Teórica, M-15, Universidad Autónoma de Madrid, E-28049 Madrid, Spain*

⁴*Instituto de Física Teórica UAM-CSIC, Universidad Autónoma de Madrid, C/ Nicolás Cabrera, 13-15, 28049 Madrid, Spain*

⁵*Galileo Galilei Institute for Theoretical Physics, Largo Enrico Fermi 2, I-50125 Firenze, Italy*

We propose a novel framework where MeV-scale Dirac Dark Matter annihilates into axion-like particles, providing a natural explanation for the 511 keV gamma-ray line observed in the Galactic Center. The relic abundance is determined by p -wave annihilation into two axion-like particles, while s -wave annihilation into three axion-like particles, decaying into e^+e^- pairs, accounts for the line intensity. Remarkably, this model, assuming a standard Navarro-Frenk-White profile, reproduces the observed emission morphology, satisfies in-flight annihilation and cosmological bounds, and achieves the correct relic density, offering a compelling resolution to this longstanding anomaly.

A prominent spectral line at 511 keV has been identified in observations of diffuse γ -ray emission at the MeV energy scale [1–3]. This emission is attributed to the annihilation of electrons and positrons forming a parapositronium (p-ps) bound state. However, the observed emission cannot be fully explained by positrons produced through cosmic-ray (CR) interactions with the interstellar medium (ISM). This discrepancy suggests evidence of an additional steady positron injection from sources located within the Galactic bulge, with a high statistical significance [4]. In addition to the 511 keV line, a continuum emission is present in the photon flux, primarily due to: *i*) the decay of the triplet ortho-positronium (o-ps) configuration, *ii*) in-flight annihilation (IfA) from the direct annihilation of positrons with ambient electrons, and *iii*) the Inverse Compton (IC) scattering of CR electrons off Galactic radiation fields. These observations indicate that positron sources significantly contribute to the diffuse γ -ray flux around \sim MeV energies [5, 6]. Various sources have been proposed in the literature, among which β -emission from radionuclides produced in massive stars appears to account for the most of the disk emission [7–9]. However, spatial morphology and injection rate of positrons in the bulge are inconsistent with known candidates, unless a unique source population with a highly concentrated central distribution is considered [10].

An appealing solution was suggested by Ref. [13]: MeV dark matter (DM) directly annihilating into e^+e^- pairs. The main motivation is that the morphology of the 511 keV emission fit quite well with the square of a Navarro-Frenk-White (NFW) DM density profile [14]. This means that, while decaying DM fails to reproduce the correct spatial morphology of the 511 keV line [15], velocity-independent DM annihilation is consistent with the observed bulge emission.

On a more specific level, to explain the Galactic Center signal, a model must satisfy three key requirements:

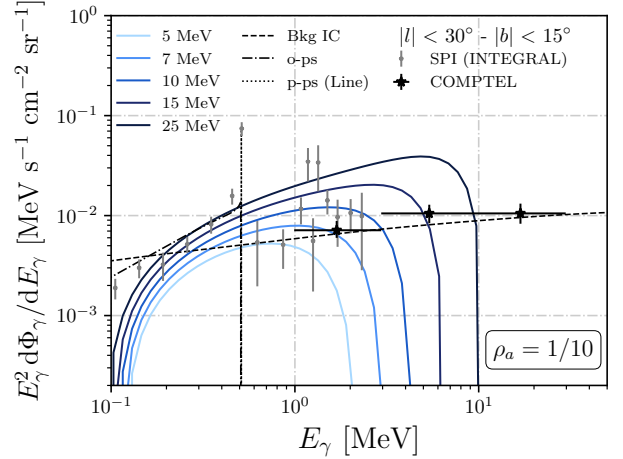


FIG. 1. The IfA emission spectrum associated with the e^+ injection from DM annihilation in our model, is presented. We consider different DM masses m_χ above 10 MeV and compare the resulting IfA signals with observations of the MeV γ -ray diffuse Galactic emission. The analysis focuses on a specific region of interest, defined as $|l| < 30^\circ$ and $|b| < 15^\circ$, where observational data from SPI (aboard INTEGRAL) [11] and COMPTEL (aboard CGRO) [12] are available. More details in the text.

i) accurately predict the total flux, *ii*) reproduce the line spectrum, and *iii*) match the observed spatial morphology of the emission. For annihilating DM, with mass m_χ , directly into e^\pm pairs, achieving the required total flux demands $\langle\sigma v\rangle/m_\chi^2 \sim 10^{-31} \text{ cm}^3 \text{ s}^{-1} \text{ MeV}^{-2}$ (see Refs. [13, 16]). Matching the line spectrum requires a DM mass below 10 MeV to avoid constraints from IC scattering and IfA. In particular, Ref. [17] demonstrated that the continuum emission from positrons capable of explaining the 511 keV signal would exceed the diffuse Galactic photon flux in the MeV range if these positrons were injected with energies above a few MeV (\sim 3 MeV).

Thus, in the simplest scenario where DM annihilates directly into e^\pm pairs, this translates into an upper limit on the DM mass. Ref. [18] revisited this analysis, softening the upper bound to approximately 7 MeV, but certainly below 10 MeV. These combined constraints on $\langle\sigma v\rangle$ and m_χ significantly restrict the parameter space, often leading to $\langle\sigma v\rangle \approx 10^{-31} \text{ cm}^3 \text{ s}^{-1}$. Such a small cross-section results in either a severe overproduction of DM in the early universe, which may potentially be avoided in models with leading p -wave annihilations, or necessitates additional annihilation channels into light products. These additional channels, however, risk conflicting with recombination and Big Bang Nucleosynthesis (BBN) constraints (see Ref. [19]). On top of this, as noted in [20], a NFW profile alone is insufficient to reproduce the observed 511 keV longitude profile when including the propagation of positrons injected with energies above ~ 10 MeV.

As a result, the straightforward explanation of thermal DM directly annihilating into e^\pm pairs has lost hype and is largely disregarded as a viable source of the excess. Additionally, more exotic DM models have been proposed, such as excited DM [21, 22], but none have yet provided a solid and natural explanation for the observed excess.

In this work, we present a novel theoretical framework in which a thermally produced light DM candidate annihilates into axion-like particles (ALPs). The subsequent decay of ALPs produces multiple e^\pm pairs, significantly reducing the kinetic energy of the injected positrons. This distinctive kinematic behavior permits DM masses exceeding 10 MeV while avoiding violations of constraints from the Galactic diffuse MeV flux. Furthermore, the model naturally accounts for both the normalization and morphology of the observed 511 keV line, remaining fully consistent with all cosmological and astronomical constraints. This provides a robust and compelling solution to a long-standing astrophysical problem.

Theoretical Framework — The model under consideration extends the Standard Model (SM) by introducing an ALP a , which couples to all three SM leptons $\ell = e, \mu, \tau$ and to a Dirac DM particle χ . Consequently, the relevant interaction Lagrangian is given by

$$\mathcal{L}_{\text{int}} \supset -ia (g_\chi \bar{\chi} \gamma_5 \chi + g_\ell \bar{\ell} \gamma_5 \ell) , \quad (1)$$

assuming that the couplings g_χ and g_ℓ are real.

We consider the mass hierarchy $2m_\chi > 3m_a > 6m_e$ where $m_\chi < 100$ MeV, which ensures that DM can produce ALPs that subsequently decay only into e^\pm at tree level and photons at loop level. As a result, the coupling to electrons g_e is the primary focus. In this mass hierarchy, the relevant annihilation processes proceed via the following t-channel mechanisms:

i) the p -wave: $\chi\bar{\chi} \rightarrow aa$,

ii) the s -wave: $\chi\bar{\chi} \rightarrow aaa$.

These two processes are entirely governed by the coupling g_χ , while the coupling g_e only affects the ALP mean-free path. If the mean-free path is smaller than the parsec scale, the two t-channel processes result in an effectively instantaneous injection of e^\pm from the perspective of the 511 keV line, with the cross section entirely determined by g_χ . Conversely, direct annihilation into e^\pm via off-shell ALP mediation does depend on the electron coupling g_e . However, since g_e is strongly constrained, as will be discussed later, the annihilation cross section into e^\pm pair via off-shell ALP mediation contributes negligibly.

In the non-relativistic limit, $s \simeq m_\chi^2(4 + \bar{v}^2)$, where \bar{v} is the DM relative velocity, the first process provides a cross section that takes the form [23, 24]:

$$\sigma v_{\chi\chi \rightarrow aa} = \frac{g_\chi^4 \bar{v}^2}{24\pi} \frac{m_\chi^2 (m_\chi^2 - m_a^2)^2}{(2m_\chi^2 - m_a^2)^4} \sqrt{1 - \frac{m_a^2}{m_\chi^2}} . \quad (2)$$

Regarding the second process, the cross section simplifies in the massless limit, $m_a \rightarrow 0$, reducing to [25]:

$$\sigma v_{\chi\chi \rightarrow aaa} \simeq \frac{(7\pi^2 - 60)g_\chi^6}{1536\pi^3 m_\chi^2} . \quad (3)$$

The more general expression with massive ALPs is given in Appendix A.

The two processes above are relevant at different stages of cosmological evolution. The p -wave channel is crucial for determining the relic density as during freeze-out the relative velocity is sufficiently high. On the other hand, the s -wave process is relevant at late time. In the massless limit, the ratio of the cross sections takes the form:

$$\eta \equiv \frac{\sigma v_{\chi\chi \rightarrow aaa}}{\sigma v_{\chi\chi \rightarrow aa}} \approx 0.23 \frac{g_\chi^2}{\bar{v}^2} . \quad (4)$$

In low-velocity environments, such as the Galactic bulge, both the phase-space and coupling suppressions in Eq. (3) are alleviated. Specifically, considering the uncertainty in the dispersion velocity of DM particles in the Galactic bulge, ranging from 50 km s^{-1} to 140 km s^{-1} [26–28], and g_χ values between 10^{-3} and 10^{-2} (consistent with thermal production, as discussed later) there exists a reasonable velocity choice such that the ratio $\eta \gg 1$ today. Consequently, the 511 keV line emission is predominantly driven by the s -wave annihilation process into three ALPs.

For this model we have taken into account the following constraints on both g_e and g_χ :

- ◇ **Thermal freeze out:** Following the approach outlined in [29], we solve the Boltzmann equation for thermal freeze-out, considering only the dominant p -wave annihilation cross section $\sigma v_{\chi\chi \rightarrow aa}$. The thermally averaged annihilation cross section is obtained by substituting \bar{v}^2 with $6/x$ where

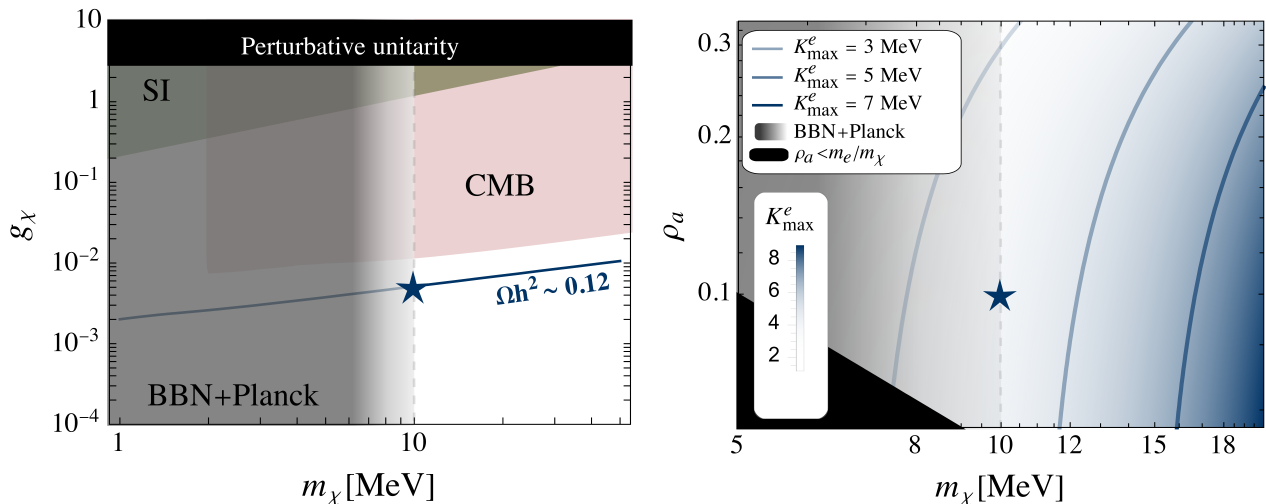


FIG. 2. **Left Panel:** Parameter space in the (m_χ, g_χ) plane, with the red, green, and black shaded regions representing the CMB, SI, and perturbative unitarity constraints, respectively. The solid blue line shows the thermal relic, while the blue star marks the thermal benchmark point with $m_\chi = 10$ MeV and $\rho_a = 1/10$. The vertical dashed gray line indicates the 2σ constraint from BBN+Planck data [19], and the gray gradient highlights regions in tension with cosmological constraints at the 3σ level (low masses). **Right panel:** Parameter space in the (m_χ, ρ_a) plane, with the maximum e^+ kinetic energy shown by an increasing blue gradient: darker blues correspond to higher values of K_{\max}^e . The three curves represent fixed values of $K_{\max}^e = 3, 5, 7$ MeV. The vertical dashed gray line, gray gradient, and blue star are the same as in the left panel. The black shaded area represents the forbidden region where $m_a < 2m_e$.

$x = m_\chi/T$ and T is the plasma temperature in Eq. (2). By requiring that $\Omega h^2 \simeq 0.12$ [30], we determine the coupling coefficient g_χ as a function of the DM mass, represented by the solid blue line in the left panel of Fig. 2. From this analysis, we find $g_\chi \approx 2 \times 10^{-3} (m_\chi/\text{MeV})^{1/2}$ with only a very small dependence on m_a within the parameter space explored in this study.

- ◇ **ALP-DM coupling:** Cosmological bounds constrain the ALP-DM coupling g_χ and we show the results in the left panel of Fig. 2. In particular data from BBN and Planck on ΔN_{eff} impose strong limits on m_χ , with [19] finding $m_\chi \lesssim 10$ MeV at 2σ confidence level (CL) for Dirac DM particle. The excluded region is represented by the gray shaded region. The CMB provides additional constraints, as DM annihilations inject energy into the plasma [31–33]. For the positron annihilation channel, we adopt the stringent bounds from [34] and the exclusion is shown as a red shaded region. Other constraints arise from the perturbative unitarity limit (black shaded region), $g_\chi < \sqrt{8\pi/3}$ [35], and DM self-interactions (SI) (green shaded region), which impose $g_\chi \lesssim 0.21 (m_\chi/\text{MeV})^{3/4}$ [36, 37].

- ◇ **ALP-electron coupling:** ALPs that couple to electrons at tree-level face various constraints discussed extensively in the literature [38–45]. In the parameter space of interest, the most strin-

gent limits arise from supernova observations, including constraints from excessive cooling and the absence of gamma-ray bursts associated with ALP decay [41]. Additional constraints are provided by beam dump experiments [44, 45]. When these constraints are combined, for ALP masses in the MeV to tens of MeV range, the allowed window for the electron coupling is $10^{-11} \lesssim g_e \lesssim 10^{-9}$, implying that $g_e \ll g_\chi$. As mentioned above, within this range of couplings, we find: *i*) DM annihilation via off-shell ALP mediation is entirely negligible, and *ii*) the ALP mean-free path is smaller than the parsec scale, ensuring an effectively instantaneous e^\pm injection for the 511 keV line signal.

As can be seen, this model is well-motivated because it allows for a thermal candidate that is not yet excluded by cosmological constraints and, as we show, reproduces the morphology of the 511 keV line.

Kinematics — The kinematics of this model, driven by the chain $\chi\bar{\chi} \rightarrow 3a \rightarrow 3(e^+e^-)$, represents a distinguishing feature compared to other DM models previously studied in the literature. The key-point of this scenario is that DM generates e^\pm with energies substantially lower than its mass. By defining $\rho_a = m_a/(2m_\chi)$, the mass hierarchy of interest corresponds to $\rho_a \in (m_e/m_\chi, 1/3)$. The differential cross-section of the injected positrons can be determined by convolving the differential cross-section for the process $\chi\bar{\chi} \rightarrow 3a$ with the energy spectrum of e^\pm resulting from the two-body decay of each ALP. We approximate the e^\pm injection spectrum using a Dirac delta

function centered at half of the ALP energy. Defining $x_{1,2} = E_{1,2}/2m_\chi$, where $E_{1,2}$ are the energies of two of the three pseudoscalars in the center-of-mass frame of the DM pair, the e^\pm injection rate per unit volume and energy, resulting from the DM annihilation process, can be expressed by the source term:

$$Q_e(\vec{x}, E_e) = \frac{1}{4} \left(\frac{\rho_\chi(\vec{x})}{m_\chi} \right)^2 \frac{1}{m_\chi} \left. \frac{d\sigma v_{\chi\chi \rightarrow aaa}}{dx_2} \right|_{x_2 = \frac{E_e}{m_\chi}}, \quad (5)$$

where further details over $d\sigma v_{\chi\chi \rightarrow aaa}/dx_2$ can be found in Appendix A. Here, we considered a generalized NFW profile [46] for the DM density, $\rho_\chi(\vec{x})$, with contraction index γ .

The positron energy spectrum is entirely governed by the parameter x_2 , which is kinematically constrained between ρ_a and $(1 - \rho_a)/2$. As a consequence, the kinetic energy range of the injected positrons is determined by

$$K_{\min}^e = \rho_a m_\chi - m_e, \quad K_{\max}^e = \frac{1 - \rho_a}{2} m_\chi - m_e. \quad (6)$$

From these equations, it follows that as $\rho_a \rightarrow 1/3$, the source term Q_e , as a function of the e^+ kinetic energy, becomes sharply peaked around $K_e = m_\chi/3 - m_e$. Conversely, as $\rho_a \rightarrow m_e/m_\chi$, Q_e broadens, with K_e spanning from zero to $(m_\chi - 3m_e)/2$. Furthermore, it is important to point out that the total cross section into three ALPs decreases as $\rho_a \rightarrow 1/3$, reaching its maximum value when $\rho_a \rightarrow m_e/m_\chi$.

In the right panel of Fig. 2 we explore the allowed parameter space in the (m_χ, ρ_a) plane, with the maximum e^+ kinetic energy shown by an increasing blue gradient. For reference, the three curves represent three fixed values of $K_{\max}^e = 3, 5, 7$ MeV. As in the left panel, the gray shaded regions indicate the Planck+BBN constraint and the black shaded region is kinematically forbidden by ALP kinematics.

We adopt hereafter $\rho_a = 1/10$ and DM masses of 10 MeV (blue stars in Fig. 2) and above. This choice ensures compliance with IfA constraints while remaining consistent with the BBN and CMB constraints. A larger scan of the parameter space is provided in Appendices C and D.

Having at our disposal the source term, we can now compute the IfA emission, upgrading the procedure described in Ref. [17] for a continuum energy spectrum at injection. In Fig. 1, we show, for different DM masses, the expected IfA emission (solid lines) in a given region of interest (longitude $|l| < 30^\circ$ and latitude $|b| < 15^\circ$), where the SPI (gray points) and COMPTEL (black points) data are available. Here we keep only the information about the peculiar spectrum of the model while the overall normalization is adjusted to reproduce the intensity of the p-ps (dotted line) line signal and the associated o-ps continuum (dot-dashed line). We also show the IC predicted background emission from CR electrons (dashed line), derived from Refs. [47, 48]. For full details, we refer the

reader to the discussion around Eq. (2.13) of Ref. [49]. We remark that low-energy data from SPI are affected by large systematic errors due to the subtraction of a relevant contribution from unresolved point sources, as discussed in [49]. Therefore, the mild overshooting of the low-energy continuum (which includes o-ps continuum, IC and IfA) does not affect our interpretation of the line signal itself. Importantly, we will show that this data-driven normalization is naturally obtained for thermal coupling and a NFW-like DM profile.

Our results indicate that the expected IfA signals are compatible with data up to a mass of approximately 15 MeV. However, introducing an additional 30% systematic uncertainty to the data, as performed in Ref. [17], would significantly relax this upper limit. Interestingly, the continuum γ -ray emission from the e^\pm produced by DM—not only the IfA emission but also the bremsstrahlung emission—could contribute to explain the apparent excess in the diffuse MeV emission observed in the inner Galaxy, as highlighted in several studies [50, 51].

In summary, the key feature of this thermal DM candidate is that positrons are injected with low energy, resulting in low IfA emission. This allows for higher DM masses to remain compatible with the measurements of the Galactic γ -ray diffuse emission.

Line Morphology— As a final step, we demonstrate that this model can reproduce the latitude (b) and longitude (l) profiles of the signal, without requiring additional non-standard astrophysical assumptions.

In order to obtain the line signal, we simulate the propagation of the low-energy leptons originating from DM annihilation by means of the DRAGON2 code [52]. This package is designed to compute all the relevant processes associated to the transport of charged particles in the Galaxy in a wide energy range, including diffusion, stochastic re-acceleration, advection, spallation and all the relevant energy losses. Our propagation setup adopts the transport parameters discussed in Ref. [53], which are derived from state-of-the-art analyses of secondary CRs in the Galaxy. More details on this computation are provided in Appendix D. We then follow the detailed prescription of Ref. [20] (see also Ref. [49]) to compute the 511 keV emission from the steady-state distribution of positrons obtained with DRAGON2.

With this result at hand, we can directly compare with the SPI observations of the spatial profiles of the emission [4]. We note that these measurements are highly dependent on the templates used to derive the data, so that extra systematic uncertainties, not well estimated and not shown in the data, are also present. However, we do not aim to give the best-fit choice of DM parameters, but to show that this DM candidate provides a satisfactory agreement with the data.

Fig. 3 shows the predicted longitude and latitude (inset panel) profiles of the 511 keV emission from annihilation of our DM candidate at a mass of 10 MeV and $\rho_a = 1/10$,

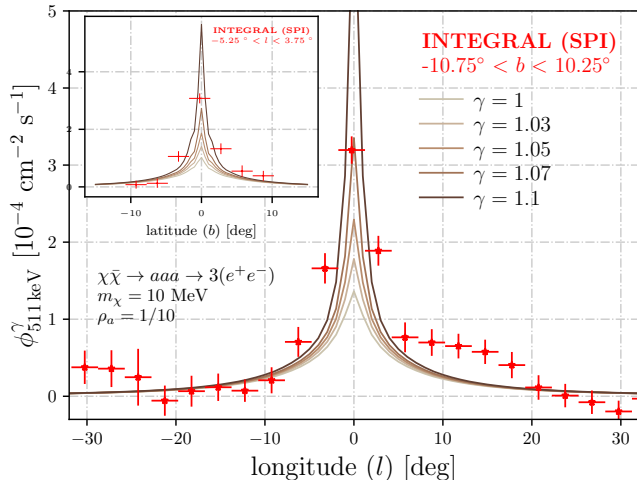


FIG. 3. Predicted longitude and latitude (inset panel) profiles for different values of the slope (γ) which represent the contraction of the DM distribution. These results correspond to the benchmark point of $m_\chi = 10$ MeV and $\rho_a = 1/10$, represented by the blue stars in Fig. 2.

for a generalized NFW DM distribution with γ ranging from 1 (standard NFW [14]) to 1.1. Remarkably, the predicted latitude and longitude profiles are able to reproduce the observed bulge-to-disk ratio for a DM distribution very close to a NFW, with no need of assuming any DM spike [49] and an astrophysical source dominating the disk emission. We show the same profiles for different masses and values of ρ_a in Fig. A3 of Appendix D. As we see from these figures, different combinations of ρ_a and the contraction index of the DM distribution allow to reproduce the profiles also for masses above 10 MeV. Moreover, we notice that different combinations of ρ_a , DM mass and DM profile would require different levels of contribution to the 511 keV line from astrophysical sources (e.g. massive stars) to explain the disk emission. We also remark that the profiles of the emission depend on the convolution of the distribution of the positrons and the density of electrons in the interstellar medium. The steeper latitude profile reflects the exponential drop of the latter above and below the Galactic plane.

Conclusions — In this letter we introduced a novel theoretical framework where a thermally produced DM candidate annihilates into ALPs. The subsequent decay of these ALPs generates multiple e^\pm pairs, producing positrons with energies significantly below the DM particle mass. This mechanism relaxes the constraints from Galactic diffuse γ -ray emission and expands the allowed DM mass range to above 10 MeV, a threshold necessary to avoid tension with cosmological observations from BBN and CMB. While DM annihilations directly into e^+e^- pairs are insufficient to account for the observed 511 keV line and the aforementioned constraints, our model provides a natural explanation for the observed 511 keV emission without requiring fine-tuning.

We found that the model, with just a single relevant parameter, is capable of simultaneously accounting for the 511 keV line and being a thermal relic. Remarkably, we observed that this model is compatible with the morphology and the bulge-to-disk emission of the observed 511 keV line, assuming a DM distribution similar to a NFW profile.

Interestingly, as detailed in Appendix C, this DM scenario predicts a significant continuum MeV emission, which could potentially explain the observed excess in MeV γ -rays [50, 51]. Additionally, the model is testable with the upcoming CMB-S4 experiment [54], offering a unique opportunity to confirm or challenge its validity.

Acknowledgements— P.D.L. is supported by the Juan de la Cierva JDC2022-048916-I grant, funded by MCIU/AEI/10.13039/501100011033 European Union "NextGenerationEU"/PRTR. The work of P.D.L. is also supported by the grants PID2021-125331NB-I00 and CEX2020-001007-S, both funded by MCIN/AEI/10.13039/501100011033 and by "ERDF A way of making Europe". P.D.L. also acknowledges the MultiDark Network, ref. RED2022-134411-T. This project used computing resources from the Swedish National Infrastructure for Computing (SNIC) under project No.2022/3-27 partially funded by the Swedish Research Council through grant no. 2018-05973. D.G. acknowledges support from the project "Theoretical Astroparticle Physics (TASP)" funded by INFN. The research conducted by M.A., A.D., G.M and P.P. receives partial funding from the European Union–Next generation EU (through Progetti di Ricerca di Interesse Nazionale (PRIN) Grant No. 202289JEW4).

Appendix A: Dark Matter annihilation

Total cross sections: As outlined in the main text, the model under consideration extends the Standard Model (SM) by introducing an axion-like particle (ALP) a that couples to all three SM leptons, $\ell = e, \mu, \tau$, as well as to a Dirac dark matter (DM) particle χ . The interaction Lagrangian for this model is provided in Eq. (1) of the main text.

Within the mass hierarchy $2m_\chi > 3m_a > 6m_e$ and for $m_\chi < 100$ MeV, DM particles can annihilate into ALPs, which subsequently decay exclusively into e^\pm pairs at tree level. The ALP-DM coupling, g_χ , fully governs the annihilation processes, while the electron coupling, g_e , primarily determines the ALP mean free path. Although g_e is tightly constrained by multiple bounds, a viable parameter space exists where the mean free path on galactic scales is sufficiently small (less than the parsec scale), while the cross-section for direct annihilation into e^\pm via off-shell ALP mediation remains negligible. As a result annihilation proceeds through the p -wave $\chi\bar{\chi} \rightarrow aa$ and the s -wave $\chi\bar{\chi} \rightarrow aaa$ processes. The Feynman diagrams for both t -channel processes are illustrated in Fig. A1.

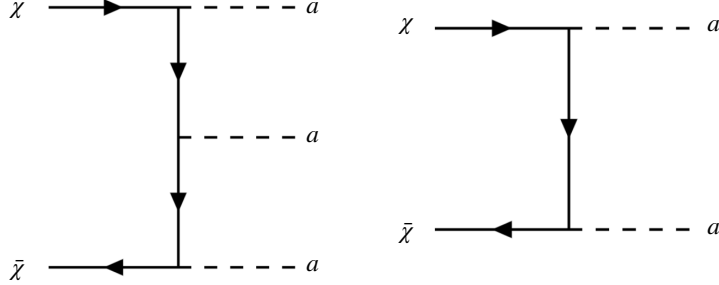


FIG. A1. Feynman diagrams for the s -wave annihilation into three pseudoscalars (*left panel*), and the p -wave into a pair of pseudoscalars (*right panel*).

Regarding the p -wave process, in the non-relativistic limit, where $s \simeq m_\chi^2 (4 + \bar{v}^2)$ and \bar{v} is the DM relative velocity, the cross section can be expressed as [23, 24]:

$$\sigma v_{\chi\bar{\chi} \rightarrow aa} = \frac{g_\chi^4 \bar{v}^2}{24\pi} \frac{m_\chi^2 (m_\chi^2 - m_a^2)^2}{(2m_\chi^2 - m_a^2)^4} \sqrt{1 - \frac{m_a^2}{m_\chi^2}}. \quad (\text{A1})$$

From [55], the full expression for the differential cross section of the s -wave process can be written as:

$$\frac{d\sigma v_{\chi\bar{\chi} \rightarrow aaa}}{dx_2} = \frac{g_\chi^6}{2^5 \cdot 3! \pi^3} \int_{x_1^{\min}}^{x_1^{\max}} dx_1 \xi(x_1, x_2, \rho_a), \quad (\text{A2})$$

where we defined the function ξ as

$$\xi(x_1, x_2, \rho_a) = \frac{(1 - 4(x_1 + x_2) + 4x_1x_2 + 4(x_1^2 + x_2^2) + 2\rho_a^2 - 3\rho_a^4)^2}{8m_\chi^2 (x_1 - \rho_a^2)^2 (x_2 - \rho_a^2)^2 (1 - x_1 - x_2 - \rho_a^2)^2}. \quad (\text{A3})$$

Here, ξ depends on $x_{1,2} = E_{1,2}/2m_\chi$, where $E_{1,2}$ are the energies of two of the three pseudoscalars in the center-of-mass frame of the DM pair, and $\rho_a = m_a/(2m_\chi)$ is constrained by the kinematics to be within $\rho_a \in (m_e/m_\chi, 1/3)$. Note that the integrand is symmetric under the exchange of x_1 and x_2 , and the integration limits are given by:

$$x_1^{\min, \max} = \frac{1 + 2x_2^2 + \rho_a^2 - x_2(3 + \rho_a^2) \mp A}{2(1 - 2x_2 + \rho_a^2)}, \quad (\text{A4})$$

where

$$A = \left[4x_2^4 - 4x_2(x_2^2 - \rho_a^2)(1 - \rho_a^2) + x_2^2(1 - 6\rho_a^2 - 3\rho_a^4) - \rho_a^2(1 - 2\rho_a^2 - 3\rho_a^4) \right]^{1/2}. \quad (\text{A5})$$

To obtain the total cross-section, Eq. (A2) must be integrated over the range of x_2 allowed by kinematics:

$$\sigma v_{\chi\bar{\chi} \rightarrow aaa} = \int_{\rho_a}^{(1-\rho_a)/2} \frac{d\sigma v_{\chi\bar{\chi} \rightarrow aaa}}{dx_2} dx_2 = \frac{g_\chi^6}{2^5 \cdot 3! \pi^3} \int_{\rho_a}^{(1-\rho_a)/2} dx_2 \int_{x_1^{\min}}^{x_1^{\max}} dx_1 \xi(x_1, x_2, \rho_a). \quad (\text{A6})$$

Remarkably, in the massless limit $m_a \rightarrow 0$, Eq. (A6) simplifies to the cross section given in [25] and in the main text:

$$\sigma v_{\chi\chi \rightarrow aaa} \simeq \frac{(7\pi^2 - 60)g_\chi^6}{1536\pi^3 m_\chi^2}. \quad (\text{A7})$$

Positron spectrum: As outlined in the previous section and in the main text, the ALP mean-free path is smaller than the parsec scale for DM masses in the MeV to tens of MeV range, ensuring an effectively instantaneous injection of e^\pm from the perspective of the 511 keV line signal. Consequently, the differential cross section for the injected positrons can be determined by convolving Eq. (A2) with the e^\pm energy spectrum arising from the two-body decay of each ALP. We approximate the e^\pm spectrum using a Dirac delta function centered at $E_2/2$. This accurately reflects the expected injection spectrum, as final state radiation is significantly suppressed at such low e^\pm energies. As a result, the differential cross section as a function of the positron energy is given by

$$\begin{aligned} \frac{d\sigma v_{\chi\chi \rightarrow aaa}}{dE_e} &= \int dx_2 \frac{d\sigma v_{\chi\chi \rightarrow aaa}}{dx_2} \delta(E_e - m_\chi x_2) = \frac{1}{m_\chi} \frac{d\sigma v_{\chi\chi \rightarrow aaa}}{dx_2} \Big|_{x_2=E_e/m_\chi} = \\ &= \frac{1}{m_\chi} \frac{g_\chi^6}{2^5 \cdot 3! \pi^3} \int_{x_1^{\min}}^{x_1^{\max}} dx_1 \xi\left(x_1, \frac{E_e}{m_\chi}, \rho_a\right). \end{aligned} \quad (\text{A8})$$

The number of positrons per annihilation event and unit energy is then obtained by dividing Eq. (A8) by the total cross section Eq. (A6):

$$\frac{d\mathcal{N}_e}{dE_e} \equiv \frac{1}{\sigma v_{\chi\chi \rightarrow aaa}} \frac{d\sigma v_{\chi\chi \rightarrow aaa}}{dE_e} = \frac{1}{m_\chi} \frac{\int_{x_1^{\min}}^{x_1^{\max}} dx_1 \xi\left(x_1, \frac{E_e}{m_\chi}, \rho_a\right)}{\int_{\rho_a}^{(1-\rho_a)/2} dx_2 \int_{x_1^{\min}}^{x_1^{\max}} dx_1 \xi(x_1, x_2, \rho_a)}. \quad (\text{A9})$$

As far as the DM spatial distribution $\rho_\chi(\vec{x})$ is concerned, we consider hereafter a generalized NFW profile. The e^\pm injection rate per unit volume and energy resulting from the DM annihilation process can be expressed by the source term:

$$Q_e(\vec{x}, E_e) = \frac{\langle\sigma v\rangle_{\chi\chi \rightarrow aaa}}{4} \left(\frac{\rho_\chi(\vec{x})}{m_\chi}\right)^2 \frac{d\mathcal{N}_e}{dE_e} \equiv \frac{1}{4} \left(\frac{\rho_\chi(\vec{x})}{m_\chi}\right)^2 \frac{1}{m_\chi} \frac{d\sigma v_{\chi\chi \rightarrow aaa}}{dx_2} \Big|_{x_2=\frac{E_e}{m_\chi}}, \quad (\text{A10})$$

where the extra factor of 1/2 compared to the standard source term for self-conjugate DM reflects the Dirac nature of the DM particle. Moreover, for s -wave processes in the non-relativistic regime, the thermally averaged cross-section is simply given by $\langle\sigma v\rangle_{\chi\chi \rightarrow aaa} = \sigma v_{\chi\chi \rightarrow aaa}$.

Appendix B: Relic Density

Following the approach outlined in [29], we solve the Boltzmann equation for thermal freeze-out, considering only the dominant p -wave annihilation cross section $\sigma v_{\chi\chi \rightarrow aa}$. The comoving number density is defined as $Y = n_\chi/s$, where n_χ is the DM number density, and s is the entropy density. Then, the Boltzmann equation becomes:

$$\frac{dY}{dz} = -\frac{s x \langle\sigma v\rangle_{\chi\chi \rightarrow aa}}{H(m_\chi)} (Y^2 - Y_{\text{eq}}^2), \quad (\text{A1})$$

where the thermally averaged annihilation cross-section $\langle\sigma v\rangle_{\chi\chi \rightarrow aa}$ is calculated by substituting $\bar{v}^2 = 6/x$, where $x = m_\chi/T$ and T is the plasma temperature, into Eq. (A1). Here, Y_{eq} represents the comoving number density at equilibrium, and $H(m_\chi)$ is the Hubble parameter evaluated at a temperature $T = m_\chi$.

For a non-relativistic relic, Eq. (A1) can be solved using a simple analytical approximation, yielding the freeze-out abundance:

$$Y_\infty \simeq \sqrt{\frac{45}{\pi}} \frac{\sqrt{g_\rho^*}}{g_s^*} \frac{1}{m_\chi M_{\text{pl}}} \left(\frac{x_{\text{fo}}}{\langle\sigma v\rangle_{\chi\chi \rightarrow aa} (2x_{\text{fo}})} \right), \quad (\text{A2})$$

TABLE I. Cross-section values $\langle\sigma v\rangle_{\chi\chi\rightarrow a\bar{a}}$ as a function of ρ_a and m_χ , expressed in cm^3s^{-1} .

	5 MeV	7 MeV	10 MeV	15 MeV	20 MeV
$\rho_a = 1/4$	4.57×10^{-32}	5.71×10^{-32}	7.37×10^{-32}	9.71×10^{-32}	1.19×10^{-31}
$\rho_a = 1/8$	1.33×10^{-31}	1.66×10^{-31}	2.14×10^{-31}	2.83×10^{-31}	3.46×10^{-31}
$\rho_a = 1/10$	1.49×10^{-31}	1.85×10^{-31}	2.40×10^{-31}	3.17×10^{-31}	3.87×10^{-31}
$\rho_a = 1/12$	1.59×10^{-31}	1.98×10^{-31}	2.56×10^{-31}	3.39×10^{-31}	4.14×10^{-31}
$\rho_a = 1/16$	1.71×10^{-31}	2.14×10^{-31}	2.76×10^{-31}	3.65×10^{-31}	4.46×10^{-31}

where g_ρ^* and g_s^* are the relativistic degrees of freedom for energy density and entropy, respectively, at a temperature $T = m_\chi$ and M_{pl} is the Planck mass. The freeze-out point x_{fo} is determined by solving the iterative equation:

$$x_{\text{fo}} = \log \left[\zeta(\zeta + 2) \sqrt{\frac{45}{8}} \frac{g_{\text{DM}} m_\chi M_{\text{pl}} \langle\sigma v\rangle_{\chi\chi\rightarrow a\bar{a}}(x_{\text{fo}})}{2\pi^3 \sqrt{g_s^* x_{\text{fo}}}} \right], \quad (\text{A3})$$

with the choice $\zeta = 1/2$ providing a good match to the full numerical solution and $g_{\text{DM}} = 4$ for a Dirac fermion.

The contribution of χ to the Universe's energy density is expressed as $\Omega = \rho_\chi/\rho_c$, where ρ_c is the critical density corresponding to a flat universe. The DM energy density, in terms of the freeze-out abundance, is given by $\rho_\chi = m_\chi s_0 Y_\infty$, with s_0 representing the present-day entropy density. By requiring $\Omega h^2 \simeq 0.12$ [30], the coupling coefficient g_χ can be determined as a function of the DM mass m_χ . We approximately obtain $g_\chi \approx 2 \times 10^{-3} (m_\chi/\text{MeV})^{1/2}$ with only a very small dependence on ρ_a within the parameter space explored in this study.

Using these results, the total s -wave cross-section is computed. Table I presents the results for different values of ρ_a and m_χ expressed in cm^3s^{-1} units.

Appendix C: In-flight annihilation emission

We evaluate the in-flight positron annihilation (IfA) signals using the approach outlined in Ref. [17], generalized to account for the fact that the e^+ injected from DM annihilations are not monochromatic but follow the spectrum described by Eq. (A9). This prescription is employed as it enables a model-independent estimation of the IfA emission, independent of propagation modeling, in a specific region of the Galaxy. The estimation is normalized to the 511 keV intensity emission observed in that region. With this normalization, the photon flux from IfA is given by

$$\frac{d\phi_{\text{IfA}}^\gamma}{d\Omega dE_\gamma} = \frac{d\phi_{511\text{ keV}}^\gamma}{d\Omega} \frac{n_{\text{H}}}{P(1 - \frac{3}{4}f)} \int_{E_\gamma}^{E_{\text{max}}} dE' \frac{1}{\mathcal{N}_e} \frac{d\mathcal{N}_e}{dE'} \int_{m_e}^{E'} P_{E'\rightarrow E} \frac{d\sigma}{dE_\gamma} \frac{dE}{|dE/dx|}, \quad (\text{A1})$$

which also depends on the electron-positron annihilation cross sections [56] (assuming a warm ionized gas) and the energy loss rate. Specifically, the second integral over E' accounts for the energy distribution of positrons injected by DM, as given in Eq. (A9), where $E_{\text{max}} = (1 - \rho_a)/2m_\chi$ and E_{min} represents the minimum positron energy required to produce γ -rays with energy E_γ . The term $(1/\mathcal{N}_e)(d\mathcal{N}_e/dE')$ represents the fraction of positrons at energy E' contributing to the 511 keV emission. The other terms describe the energy loss for a positron with energy E' before annihilation, the number density of electrons n_{H} including both bound electrons within hydrogen atoms and free electrons (which determine the number of targets for positron scattering), and the probability $P_{E'\rightarrow E}$ (from Eq. (4) of Ref. [17]), which gives the likelihood per unit energy for a positron with initial energy E' to produce a γ -ray in flight before reaching energy E . Additionally, $P = P_{E'\rightarrow m_e}$ represents the probability for a positron with initial energy E' to produce a photon before thermalizing, and $f = 0.967 \pm 0.022$ [57] is the fraction of positrons annihilating through positronium states.

In the region of interest of SPI and COMPTEL data (*i.e.* latitude $|b| < 15^\circ$ and longitude $|l| < 30^\circ$), the line peak flux is $d\phi_{511\text{ keV}}^\gamma/d\Omega = 0.07 \text{ MeV cm}^{-2} \text{ s}^{-1} \text{ sr}^{-1}$, as can be seen in Fig. A2. In the left panel of this figure, we present the IfA continuum signals from the annihilation of conventional DM (direct annihilation into an e^\pm pair) for different DM mass values. In the right panel, we show the IfA emission predicted by our model, fixing the DM mass at $m_\chi = 10 \text{ MeV}$ and varying ρ_a . Here, it is evident that IfA emissions are not significantly affected by variations in ρ_a . This behavior is also observed for other choices of DM mass. In both panels, the intensities of the 511 keV line and

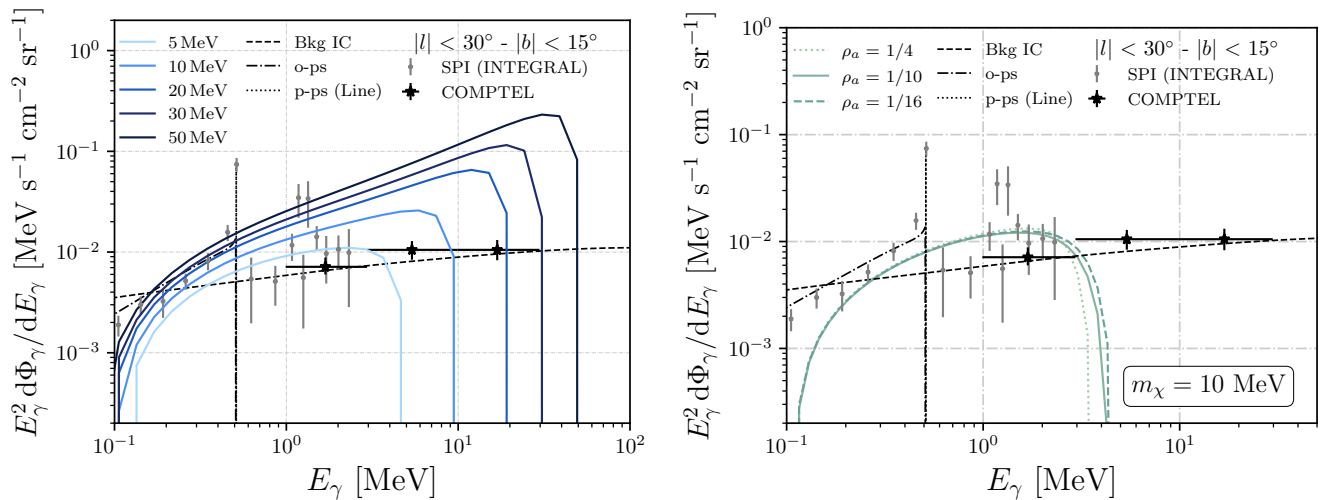


FIG. A2. **Left panel:** Predicted IfA signals from DM annihilating in the conventional scenario (i.e. injecting monoenergetic positrons), for different DM masses. **Right panel:** Expected IfA signal expected for a 10 MeV DM particle for different values of ρ_a .

the associated ortho-positronium continuum emissions are shown as dotted and dot-dashed black lines, respectively, while the signal from the IC background is represented by a dashed black line.

The comparison between the left panel of Fig. A2 and Fig. 1 in the main text highlights the improvement of our model over the conventional DM scenario, which already forbids a DM mass of 10 MeV. Conversely, the IfA emission predicted by our model is compatible with COMPTEL and SPI data.

We also remark that models of CR electrons tuned on Voyager-1 data, fail to reproduce the γ -ray emission in the inner Galaxy at MeV energies. Remarkably, the leptons produced within our scenario could help to explain the apparent excess [50, 51]. However, this anomaly can be avoided considering models [47, 48], that are only constrained by AMS-02 data and Fermi-LAT local emissivity measurements.

Appendix D: Line morphology: Numerical Setup and Parameter Variations

In order to obtain the line signal, we need to calculate numerically the distribution of the positrons, originating from DM annihilation, after propagation in the interstellar medium. To this aim, we use the DRAGON code [52], a numerical package designed to compute all the physical processes associated to the transport of charged particles in the Galaxy including diffusion, stochastic reacceleration, advection, spallation, and energy losses.

Regarding the latter, which is the most relevant for MeV electrons/positrons, DRAGON can realistically take into account inverse Compton scattering, synchrotron emission, bremsstrahlung, ionization and Coulomb scattering, embedding up-to-date models for the distribution of the astrophysical targets of interest for each process. We remark that, in the energy domain we are focusing on, the timescales associated to Coulomb and ionization losses are by far the dominant ones (see for instance the discussion in [58] for more details): hence, the large uncertainties due to the details of diffusive transport have little impact on our final result.

Once all the relevant processes are correctly initialized, the injection of charged leptons associated to our DM model is implemented as in Eq. A10. The charged particles are then propagated in a two-dimensional cylindrically symmetric spatial grid with spacing $\simeq 100$ pc, which is appropriate to resolve the spatial variations of the energy loss term. The kinetic energy range under consideration is [100 eV - 100 MeV]. The convergence is reached adopting a variable timestep with a maximum value of $\delta t = 64$ Myr and a minimum value of $\delta t = 100$ y, which is appropriate to cover the different timescale involved in the problem. We adopt the propagation parameters discussed in Ref. [53], derived from state-of-the-art analyses of secondary cosmic rays in the Galaxy. The runs are available at <https://doi.org/10.5281/zenodo.10076728>.

With the propagated flux of charged leptons at hand, the 511 keV line flux integrated along the line of sight (where

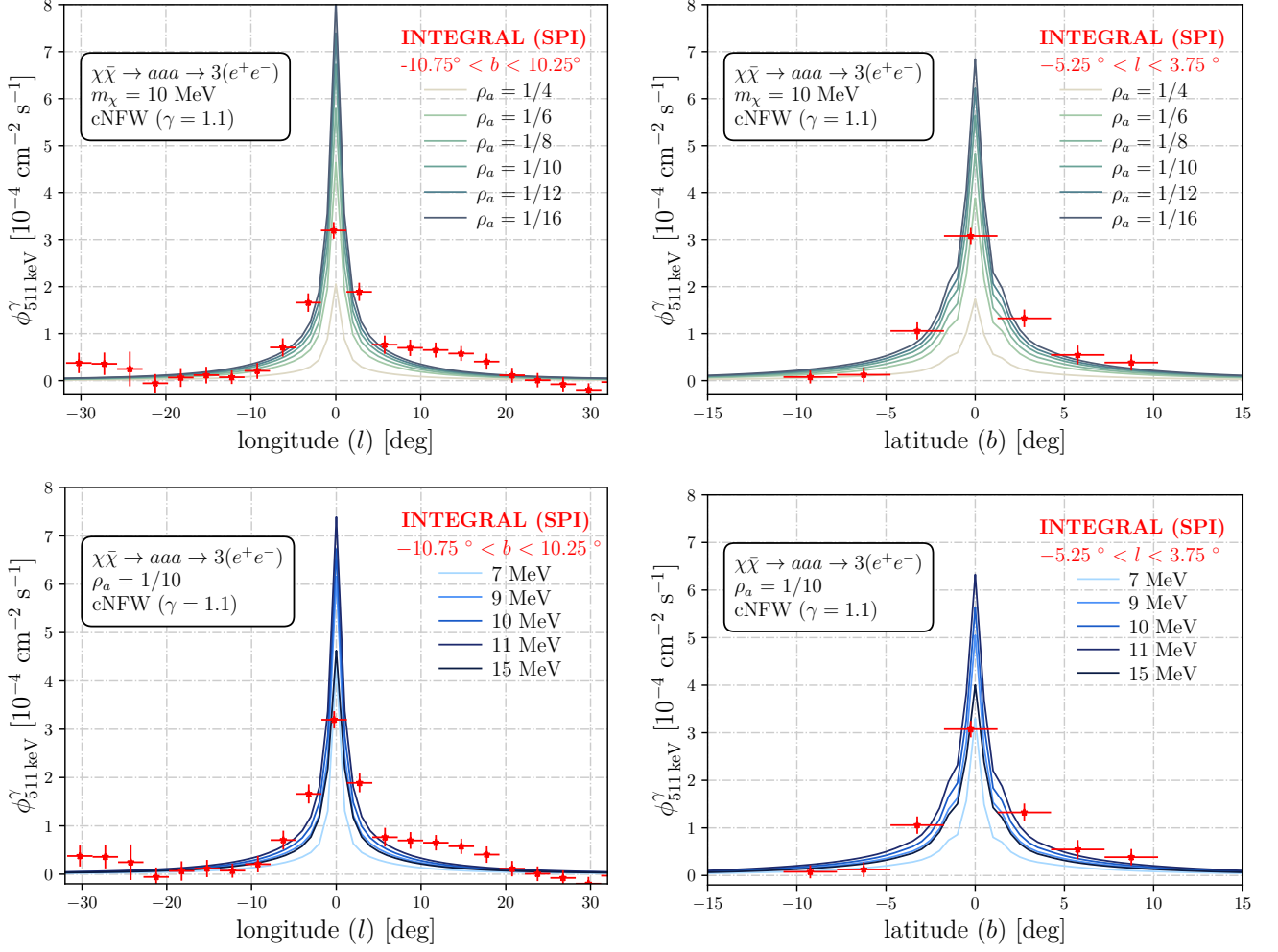


FIG. A3. **Top row:** Longitude profile (*left panel*) and latitude (*right panel*) for different values of ρ_a and a DM mass of 10 MeV, adopting a cNFW ($\gamma = 1.1$) DM distribution. **Bottom row** Longitude (*left panel*) and latitude (*right panel*) profiles for different DM masses, at $\rho_a = 1/10$ and adopting a cNFW ($\gamma = 1.1$) DM distribution.

the variable s runs) is expressed as follows (for more details, see Ref. [49]):

$$\frac{d\phi_{511\text{keV}}^\gamma}{d\Omega} = 6k_{\text{ps}} \int_{\text{l.o.s.}} ds \left(\frac{d\phi^{e^+}}{d\Omega} \right)_{\text{propagated}} n_e \cdot \sigma_{\text{ann}}(E_{\text{th}}), \quad (\text{A1})$$

where: $k_{\text{ps}} = 1/4$ is the fraction of positronium decays contributing to the 511 keV line signal, the factor 6 accounts for the emission of two 511 keV photons per positronium annihilation times three positrons injected per DM annihilation in the process $\chi\chi \rightarrow aaa \rightarrow 3(e^+e^-)$, n_e is the free electron density, and σ_{ann} the cross section of positron annihilation at the energy of the thermalized positrons E_{th} . We consider the thermal energy of a warm medium (with $T = 8000$ K), as suggested by Ref. [59]. This implies that the main annihilation cross section is the direct electron-positrons annihilation [60].

Let us now present how the results obtained within this setup vary with respect to the choice of the most relevant parameters. In the top row of Fig. A3 we show the expected longitude (*left panel*) and latitude (*right panel*) profiles for different values of ρ_a (keeping the DM mass fixed at 10 MeV), for a contracted NFW (c-NFW) with contraction index $\gamma = 1.1$. The differences in normalization arise from the direct dependence of the annihilation rate on ρ_a . Additionally, varying ρ_a slightly influences the morphology of the expected signal. In most cases considered here, the SPI data can be accurately reproduced. In the bottom row of the figure, we compare the longitude (*left panel*) and latitude (*right panel*) profiles predicted for different DM masses at $\rho_a = 1/10$, assuming a contracted NFW

(c-NFW) profile with a contraction index $\gamma = 1.1$. For various parameter choices, the SPI profiles are well-matched, demonstrating the capability of the proposed model to potentially address a longstanding astrophysical puzzle.

-
- [1] I. Johnson, W. N., J. Harnden, F. R., and R. C. Haymes, *The Astrophysical Journal Letters* **172**, L1 (1972).
- [2] I. Johnson, W. N. and R. C. Haymes, *The Astrophysical Journal* **184**, 103 (1973).
- [3] M. Leventhal, C. J. MacCallum, A. F. Hutters, and P. D. Stang, *Astrophys. J.* **302**, 459 (1986).
- [4] T. Siebert *et al.*, *Astron. Astrophys.* **586**, A84 (2016), arXiv:1512.00325 [astro-ph.HE].
- [5] R. M. Bandyopadhyay, J. Silk, J. E. Taylor, and T. J. Maccarone, *Monthly Notices of the Royal Astronomical Society* **392**, 1115 (2009).
- [6] F. W. Stecker, *apss* **3**, 579 (1969).
- [7] N. Prantzos, C. Boehm, A. M. Bykov, R. Diehl, K. Ferrière, N. Guessoum, P. Jean, J. Knoedlseder, A. Marcowith, I. V. Moskalenko, A. Strong, and G. Weidenspointner, *Rev. Mod. Phys.* **83**, 1001 (2011).
- [8] J. Knödlseder, P. Jean, V. Lonjou, G. Weidenspointner, N. Guessoum, W. Gillard, G. Skinner, P. von Ballmoos, G. Vedrenne, J.-P. Roques, S. Schanne, B. Teegarden, V. Schönfelder, and C. Winkler, *Astronomy & Astrophysics* **441**, 513–532 (2005).
- [9] G. Weidenspointner *et al.*, *Astron. Astrophys.* **450**, 1012 (2006), arXiv:astro-ph/0601673.
- [10] R. Bartels, F. Calore, E. Storm, and C. Weniger, *Mon. Not. Roy. Astron. Soc.* **480**, 3826 (2018), arXiv:1803.04370 [astro-ph.HE].
- [11] L. Bouchet, A. W. Strong, T. A. Porter, I. V. Moskalenko, E. Jourdain, and J.-P. Roques, *Astrophys. J.* **739**, 29 (2011), arXiv:1107.0200 [astro-ph.HE].
- [12] A. W. Strong, K. Bennett, H. Bloemen, R. Diehl, W. Hermsen, D. Morris, V. Schoenfelder, J. G. Stacy, C. de Vries, M. Varendorff, C. Winkler, and G. Youssefi, *A&A* **292**, 82 (1994).
- [13] C. Boehm *et al.*, *Phys. Rev. Lett.* **92**, 101301 (2004), arXiv:astro-ph/0309686.
- [14] J. F. Navarro, C. S. Frenk, and S. D. M. White, *The Astrophysical Journal* **462**, 563 (1996).
- [15] C. Boehm, D. Hooper, J. Silk, M. Casse, and J. Paul, *Physical Review Letters* **92** (2004), 10.1103/physrevlett.92.101301.
- [16] R. J. Wilkinson, A. C. Vincent, C. Boehm, and C. McCabe, *Physical Review D* **94** (2016), 10.1103/physrevd.94.103525.
- [17] J. F. Beacom and H. Yüksel, *Physical Review Letters* **97** (2006), 10.1103/physrevlett.97.071102.
- [18] P. Sizun, M. Cassé, S. Schanne, and B. Cordier, “Constraints on the injection energy of positrons in the galactic centre region,” (2007), arXiv:astro-ph/0702061 [astro-ph].
- [19] N. Sabti, J. Alvey, M. Escudero, M. Fairbairn, and D. Blas, *Journal of Cosmology and Astroparticle Physics* **2020**, 004–004 (2020).
- [20] P. De la Torre Luque, S. Balaji, and J. Silk, *Astrophys. J. Lett.* **973**, L6 (2024), arXiv:2312.04907 [hep-ph].
- [21] H. An, M. Pospelov, and J. Pradler, *AIP Conference Proceedings* **1534**, 23 (2013), https://pubs.aip.org/aip/acp/article-pdf/1534/1/23/11626914/23_1_online.pdf.
- [22] C. V. Cappiello, M. Jafs, and A. C. Vincent, *Journal of Cosmology and Astroparticle Physics* **2023**, 003 (2023).
- [23] C. Arina, E. Del Nobile, and P. Panci, *Phys. Rev. Lett.* **114**, 011301 (2015), arXiv:1406.5542 [hep-ph].
- [24] G. Armando, P. Panci, J. Weiss, and R. Ziegler, *Physical Review D* **109** (2024), 10.1103/physrevd.109.055029.
- [25] F. Kahlhoefer, K. Schmidt-Hoberg, and S. Wild, *Journal of Cosmology and Astroparticle Physics* **2017**, 003–003 (2017).
- [26] S. K. Kataria and M. Das, *The Astrophysical Journal* **886**, 43 (2019).
- [27] E. Valenti, M. Zoccali, A. Mucciarelli, O. A. Gonzalez, F. Surot, D. Minniti, M. Rejkuba, L. Pasquini, G. Fiorentino, G. Bono, R. M. Rich, and M. Soto, *Astronomy & Astrophysics* **616**, A83 (2018).
- [28] K. Gültekin, D. O. Richstone, K. Gebhardt, T. R. Lauer, S. Tremaine, M. C. Aller, R. Bender, A. Dressler, S. M. Faber, A. V. Filippenko, R. Green, L. C. Ho, J. Kormendy, J. Magorrian, J. Pinkney, and C. Siopis, *The Astrophysical Journal* **698**, 198–221 (2009).
- [29] G. Servant and T. M. Tait, *Nuclear Physics B* **650**, 391–419 (2003).
- [30] Planck Collaboration, *Astronomy & Astrophysics* **641**, A6 (2020), arXiv:1807.06209 [astro-ph.CO].
- [31] P. J. E. Peebles, S. Seager, and W. Hu, *Astrophys. J. Lett.* **539**, L1 (2000), arXiv:astro-ph/0004389.
- [32] X.-L. Chen and M. Kamionkowski, *Phys. Rev. D* **70**, 043502 (2004), arXiv:astro-ph/0310473.
- [33] N. Padmanabhan and D. P. Finkbeiner, *Phys. Rev. D* **72**, 023508 (2005).
- [34] T. R. Slatyer, *Phys. Rev. D* **93**, 023527 (2016).
- [35] C. Cornella, P. Paradisi, and O. Sumensari, *Journal of High Energy Physics* **2020** (2020), 10.1007/jhep01(2020)158.
- [36] S. Tulin, H.-B. Yu, and K. M. Zurek, *Phys. Rev. D* **87**, 115007 (2013).
- [37] D. N. Spergel and P. J. Steinhardt, *Physical Review Letters* **84**, 3760–3763 (2000).
- [38] D. J. E. Marsh, *Phys. Rept.* **643**, 1 (2016), arXiv:1510.07633 [astro-ph.CO].
- [39] M. Bauer, M. Neubert, and A. Thamm, *JHEP* **12**, 044 (2017), arXiv:1708.00443 [hep-ph].
- [40] I. G. Irastorza and J. Redondo, *Prog. Part. Nucl. Phys.* **102**, 89 (2018), arXiv:1801.08127 [hep-ph].
- [41] R. Z. Ferreira, M. C. D. Marsh, and E. Müller, *JCAP* **11**, 057 (2022), arXiv:2205.07896 [hep-ph].
- [42] D. Ghosh and D. Sachdeva, *JCAP* **10**, 060 (2020), arXiv:2007.01873 [hep-ph].
- [43] P. F. Depta, M. Hufnagel, and K. Schmidt-Hoberg, *JCAP* **04**, 011 (2021), arXiv:2011.06519 [hep-ph].
- [44] R. Essig, R. Harnik, J. Kaplan, and N. Toro, *Phys. Rev. D* **82**, 113008 (2010).

- [45] J. D. Bjorken, S. Ecklund, W. R. Nelson, A. Abashian, C. Church, B. Lu, L. W. Mo, T. A. Nunamaker, and P. Rassmann, *Phys. Rev. D* **38**, 3375 (1988).
- [46] H. Zhao, *MNRAS* **278**, 488 (1996), arXiv:astro-ph/9509122 [astro-ph].
- [47] P. de la Torre Luque *et al.*, *JCAP* **07**, 008 (2022), arXiv:2202.03559 [astro-ph.HE].
- [48] P. De la Torre Luque, F. Loparco, and M. N. Mazziotta, *JCAP* **10**, 011 (2023), arXiv:2305.02958 [astro-ph.HE].
- [49] P. De la Torre Luque, S. Balaji, M. Fairbairn, F. Sala, and J. Silk, Under review in *JCAP* (2024), arXiv:2410.16379 [astro-ph.HE].
- [50] C. M. Karwin, T. Siegert, J. Beechert, J. A. Tomsick, T. A. Porter, M. Negro, C. Kierans, M. Ajello, I. Martinez-Castellanos, A. Shih, A. Zoglauer, and S. E. Boggs, *The Astrophysical Journal* **959**, 90 (2023).
- [51] E. Orlando, *Monthly Notices of the Royal Astronomical Society* **475**, 2724–2742 (2017).
- [52] C. Evoli, D. Gaggero, A. Vittino, G. Di Bernardo, M. Di Mauro, A. Ligorini, P. Ullio, and D. Grasso, *JCAP* **02**, 015 (2017), arXiv:1607.07886 [astro-ph.HE].
- [53] P. De la Torre Luque, S. Balaji, and J. Koechler, *Astrophys. J.* **968**, 46 (2024), arXiv:2311.04979 [hep-ph].
- [54] K. Abazajian *et al.*, “Cmb-s4 science case, reference design, and project plan,” (2019), arXiv:1907.04473 [astro-ph.IM].
- [55] N. F. Bell, Y. Cai, J. B. Dent, R. K. Leane, and T. J. Weiler, *Physical Review D* **96** (2017), 10.1103/physrevd.96.023011.
- [56] P. A. M. Dirac, *Mathematical Proceedings of the Cambridge Philosophical Society* **26**, 361–375 (1930).
- [57] P. Jean, J. Knödlseeder, W. Gillard, N. Guessoum, K. Ferrière, A. Marcowith, V. Lonjou, and J. P. Roques, *Astronomy & Astrophysics* **445**, 579–589 (2005).
- [58] R. Bartels, D. Gaggero, and C. Weniger, *JCAP* **05**, 001 (2017), arXiv:1703.02546 [astro-ph.HE].
- [59] J. Knödlseeder, P. Jean, V. Lonjou, G. Weidenspointner, N. Guessoum, W. Gillard, G. Skinner, P. von Ballmoos, G. Vedrenne, J.-P. Roques, S. Schanne, B. Teegarden, V. Schönfelder, and C. Winkler, *Astronomy & Astrophysics* **441**, 513–532 (2005).
- [60] N. Guessoum, R. Ramaty, and R. E. Lingenfelter, *Astrophys. J.* **378**, 170 (1991).